# Natural Convection in Enclosures with Periodic Spatial Heating

**Mirza Faisal Baig** and **Nadeem Hasan**

*Dept. of Mechanical Engineering*
*Aligarh Muslim University,*
*Aligarh, India-202002*

**Abstract:** The purpose of this numerical study is to study the spatio-temporal dynamics of an incompressible Bousinessq, low Prandtl number (Pr=7) fluid confined in a two-dimensional enclosure. The non-dimensional equations in primitive variables that govern the transport of mass, momentum and heat have been solved numerically using second and fifth-order accurate upwinding in space and first order accuracy in time. Due to the non-linearity of thermal boundary conditions, introduced by spatially discrete periodic heating and insulation, spatial asymmetricity in pattern of streamline rolls and isotherms as well as temporal asymmetricity in the form of quasi-periodicity appears at lower Rayleigh number compared to standard Rayleigh-Benard problem. The density circulation effect gets enhanced with increasing Rayleigh numbers and this in turn significantly reduces the vertical heat transport as well as results in breaking up of alternately larger and smaller rolls into a multicellular convection.

## INTRODUCTION

Most of the researchers have investigated the standard Rayleigh-Benard (R-B) phenomenon either in cubical enclosures or circular cylinder enclosures with absolutely uniform temperatures on the top and bottom horizontal boundaries. The fixed boundary condition of temperature has been studied in detail by various researchers, both experimentally by Koschmeider [1], Gollub and Benson [2], Behringer and Ahlers [3], etc and numerically by Curry et. al.[4], Mukutmoni and Yang [5], Stella et. al. [6] etc. Both Gollub and Benson [2] and Mukutmoni and Yang [5] found that the preferred route of transition from laminar to chaotic state is Ruelle, Takens and Newhouse [7] route if asymmetric boundary conditions are maintained and Feigenbaums' [8] period doubling route if special symmetry conditions are imposed numerically.

The presence of systematic non-uniformities on the horizontal boundary produces a horizontal pressure gradient in the fluid, because the hydrostatic pressure under a warm fluid column is smaller than the hydrostatic pressure under a cold fluid column of same depth. That means the fluid will move from higher pressure to lower pressure regions, independent of the magnitude of the vertical temperature gradient, even with stable stratification. So the circulation generated by the vertical temperature gradient will be

nonlinearly superimposed on the density circulation, which finally introduces an orientation into the fluid layer which is likely to change the scenario of the patterns that one finds on a uniformly heated plane.

The investigation of convection with non-uniform heating began with an experiment of Koschmeider [9]. The axisymmetric radial temperature gradient on bottom plane results in circulation given by the pressure differences between the warm and cold fluid columns. As vertical instability is also present in a non-uniformly heated fluid layer, each second convection roll will turn in a direction opposite to the motion of the density circulation; each second roll is therefore smaller than its neighbor which turns with the density circulation. This pattern of rolls persists till moderately supercritical conditions.

Further rise in radial temperature gradient results in convection rolls changing the orientation of their axes from the azimuthal to radial direction. The only other two experimental investigations of R-B convection with non-uniform temperature on the horizontal boundaries are from Berkovsky and Fertman [10] and Srulijes [11], both made with rectangular containers. In Srulijes [11] experiments on the top as well as bottom boundaries had the same linear horizontal temperature gradient and resulted in pattern of alternately larger and smaller rolls. Weber [12,13] studied theoretically the two dimensional case with a constant $\partial\theta/\partial x$ on the bottom and a uniform $\theta$ on top wall, assuming $|\partial\theta/\partial x| << |\partial\theta/\partial y|$. He showed that the onset of convection in the presence of a horizontal temperature gradient will take place at a Ra number larger than the critical Ra on a uniformly heated plane, attributing this to the density circulation which reduces the vertical temperature gradient and thus making the fluid layer more stable.

Our aim of investigation was to observe the spatio-temporal changes in a square enclosure with increasing Ra number but also to analyze the character of transition from laminar to highly aperiodic natural convection that occurs in the presence of discrete spatially periodic heating on the bottom horizontal plane, which introduces a nonlinear horizontal temperature gradient. To the present knowledge of authors, this type of boundary condition has not been investigated by any researcher. In section 2 we summarize the dynamical equations and numerical scheme employed in our analysis. In section 3 the states of medium Pr number (Pr=7.0) 2D convection are studied. In section 4 conclusions are drawn and future scope of work discussed.

## MATHEMATICAL FORMULATION

The non-dimensional equations in primitive variables that govern the transport of mass, momentum and heat in an incompressible Bousinessq fluid can be written in weak conservative form in a two-dimensional Cartesian coordinate system as

$$\partial u/\partial x + \partial v/\partial y = 0 \quad (1)$$

$$\partial u/\partial t + \partial u^2/\partial x + \partial uv/\partial y = -\partial p/\partial x + Pr\,\nabla^2 u \quad (2)$$

$$\partial v/\partial t + \partial uv/\partial x + \partial v^2/\partial y = -\partial p/\partial y + Pr\nabla^2 v + Ra\,Pr\,\theta \quad (3)$$

$$\partial\theta/\partial t + \partial u\theta/\partial x + \partial v\theta/\partial y = \nabla^2\theta \quad (4)$$

The Poisson equation for pressure is given as

$$\nabla^2 p = - \partial D/\partial t - 2\,\partial^2 uv/\partial x\partial y - \partial^2 u^2/\partial x^2 - \partial^2 v^2/\partial y^2 + Pr\,\nabla^2 D + Ra\,Pr\,\partial\theta/\partial y \qquad (5)$$

where $Ra = \alpha g H^3 \Delta T/\nu\kappa$. The flow is assumed to occur in a square enclosure in the region $0 \le x \le H$ and $0 \le y \le H$. The reference length, velocity and time used are H, $\kappa/H$ and $H^2/\kappa$.

No-slip boundary conditions are employed for u and v on all the walls. $\theta$ is assumed to satisfy conducting boundary conditions on the top and discrete portions of bottom heated plate, while the Neumann boundary condition $\partial\theta/\partial x = 0$ is assumed for the insulated side walls (see Fig.1). The perturbation in temperature in the fluid is provided by the temperature gradient due to unit time the fluid needs to acquire the adjacent wall temperature. The boundary conditions used are :

| | |
|---|---|
| $\theta = 1.0$ | on portions AB, CD and EF (heating portions) |
| $\partial\theta/\partial y = 0.0$ | on portions BC and DE (non heating portions) |
| $\theta = 0.0$ | on top wall GH |
| $\partial\theta/\partial x = 0.0$ | on vertical walls AH and GF |
| u,v = 0.0 | on all the walls |

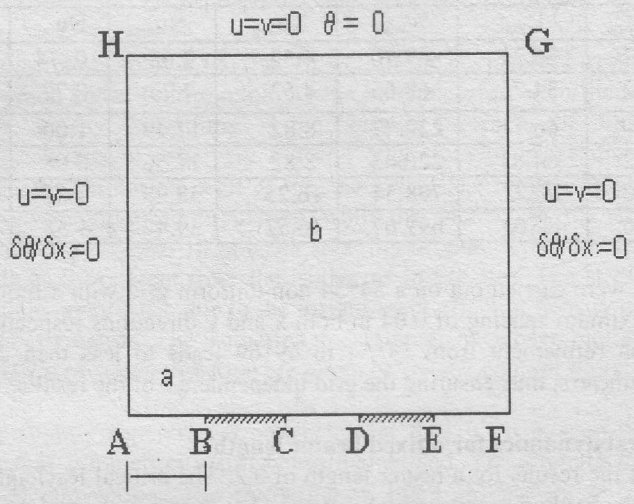


Fig. 1 Physical domain of the problem.

The nonlinear terms in eqns. (2) to (4) are evaluated using second order upwinding in space i.e. Leonard's [14] QUICK scheme or fifth-order upwinding as used by Rai and Moin [15]. The diffusion terms are discretized using the three point central differencing stencil, while the time integration has been performed explicitly (Euler's scheme) in order to capture the unsteady physics especially of the oscillatory flow regime. The Poisson eqn. for pressure (5) has been solved using Strongly Implicit Procedure (SIP) till a $L_2$-norm tolerance limit of $10^{-6}$ is reached (for non-dimensional pressure values of the order of

$10^{12}$). The above method has been implemented on a 54*54 orthogonal, non-uniform, collocated mesh with a minimum and maximum grid spacing of 0.004 and 0.04 in either directions respectively. The time integration was performed for 100 to 250 seconds in physical time using a variable dimensional time step of order of $10^{-5}$ at low Ra flows and $10^{-6}$ — $10^{-7}$ at high Ra flows. The time histories of dynamical variables like u,v and θ are recorded at two points shown as (a) and (b) in fig. 1. The coordinates for these points are (0.1, 0.1) and (0.5, 0.5) respectively.

For spectral analysis of time series data, codes were developed to calculate power spectrum using Entropy method, Press et al. [16] and Phase Portraits as given in Gollub and Baker [17], etc.

## TIME DEPENDENT CONVECTION

The developed code has been validated with the numerical results of Nonino et.al [18] for 2D differentially heated square cavity problem and an error in between 1-2% is obtained for velocities and Nusselt numbers at the heated wall for Ra=$10^5$ to $10^7$ as shown in Table 1.

Table 1. Validation of code with numerical results of C. Nonino et. al[18]

| Ra | $\|\psi\|_{max}$ | $U_{max}$ | $V_{max}$ | $Nu_{avg}$ | $Nu_{max}$ | $Nu_{min}$ | Reference |
|---|---|---|---|---|---|---|---|
| $10^5$ | 9.67 | 35.21 | 69.10 | 4.52 | 7.68 | 0 .74 | present |
| $10^5$ | 9.62 | 34.75 | 68.65 | 4.52 | 7.73 | 0.72 | [18] |
| $10^6$ | 16.89 | 66.11 | 222.77 | 8.82 | 17.49 | 1.00 | present |
| $10^6$ | 16.82 | 64.83 | 220.63 | 8.82 | 17.56 | 0.98 | [18] |
| $10^7$ | 31.40 | 152.23 | 708.54 | 16.25 | 38.98 | 1.38 | present |
| $10^7$ | 30.16 | 148.60 | 699.67 | 16.52 | 39.47 | 1.38 | [18] |

The validations were carried out on a 54*54 non-uniform grid with a minimum spacing of 0.004 and a maximum spacing of 0.04 in both x and y directions respectively. It has been found that mesh refinement from 54*54 to 69*69 leads to less than 2% deviation for benchmark parameters, thus ensuring the grid independence of the results.

### Spatio-Temporal dynamics for a fixed heater length

First we present the results for a heater length of 0.2. The critical Rayleigh number $Ra_c$ is obtained using the method proposed by Silveston [19] where a change in non-dimensional heat flux curve i.e. the change in slope of Nusselt number vs Ra number curve gives a value in the vicinity of 3700 as shown in Fig.2. The higher value of $Ra_c$ is consistent with the findings of Koschmeider [9] for similar non-uniform heating boundary conditions. Fig 3(a)-3(g) depict instantaneous snapshots of isotherms and streamlines in the flow field. The flow attains a steady state for Ra=$10^3$ and Ra=$10^4$. Therefore the flow fields depicted in figures 3(a) and 3(b) are steady flow fields. For Ra > $10^4$ not only the instantaneous snapshots but also the flow field development in the form of streamline patterns at different instants of time for a given Ra and heater length $H_l$ = 0.2 are shown in figures 4(a)-4(e).

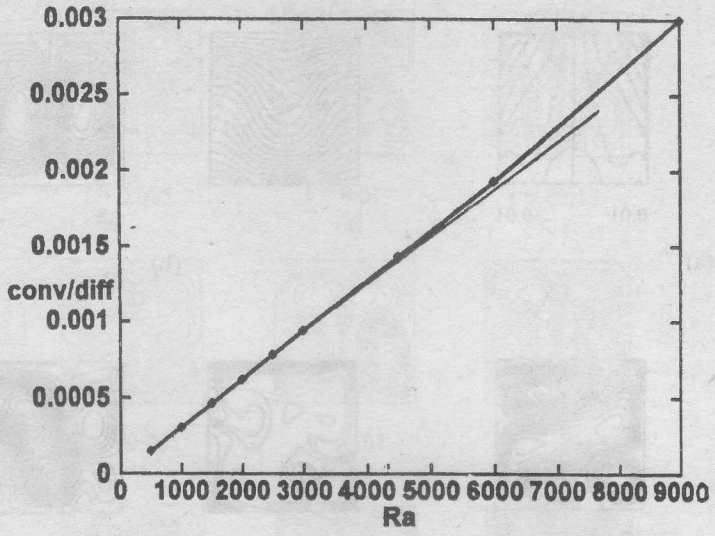


Fig. 2 Evaluation of critical Rayleigh number.

Because of the discrete heating at the bottom wall of the enclosure, there are two principal driving forces which cause fluid motion: 1) the buoyancy forces in the vertical direction induced due to density variations, 2) the pressure forces in the horizontal direction induced due to columns of relatively hot and cold fluid over the discrete heated and insulated portions of the bottom wall of the enclosure. The motion induced by former is referred to as buoyancy induced circulation, while that induced by the latter is referred to as density circulation. At $Ra=10^3$ i.e. at subcritical conditions, the conduction is the 4dominant mode as is apparent from the isotherms in Fig.3(a). The streamline pattern in Fig. 3(a) is spatially symmetric due to the insignificant effect of density circulation on the buoyancy driven circulation. The isotherms in all figures have been plotted in the range of 0 — 1.0. The ranges of stream function are given below the contour plots.

In fig 3(b), for slightly supercritical convection at $Ra=10^4$, it is seen that two rolls are formed with spatial symmetricity still being maintained. The strength of rolls is greater due to increased convection. The isotherms in Fig.3 (b) are more curved signifying increased convective motion. From the point of view of temporal behavior the flow evolves into a steady state at this Ra.

Fig 4 shows the snapshots of streamline patterns at different instants of time with increasing Ra number for $H_1 = 0.2$. It is particularly evident from fig. 4d and fig. 4e that initially the convection is driven by the vertical forces of gravity with the streamline pattern being highly multicellular and at a later stage, as the horizontal density gradients build up in flow, the convection is driven by density circulation with an almost single dominant convective roll with minor secondary rolls.

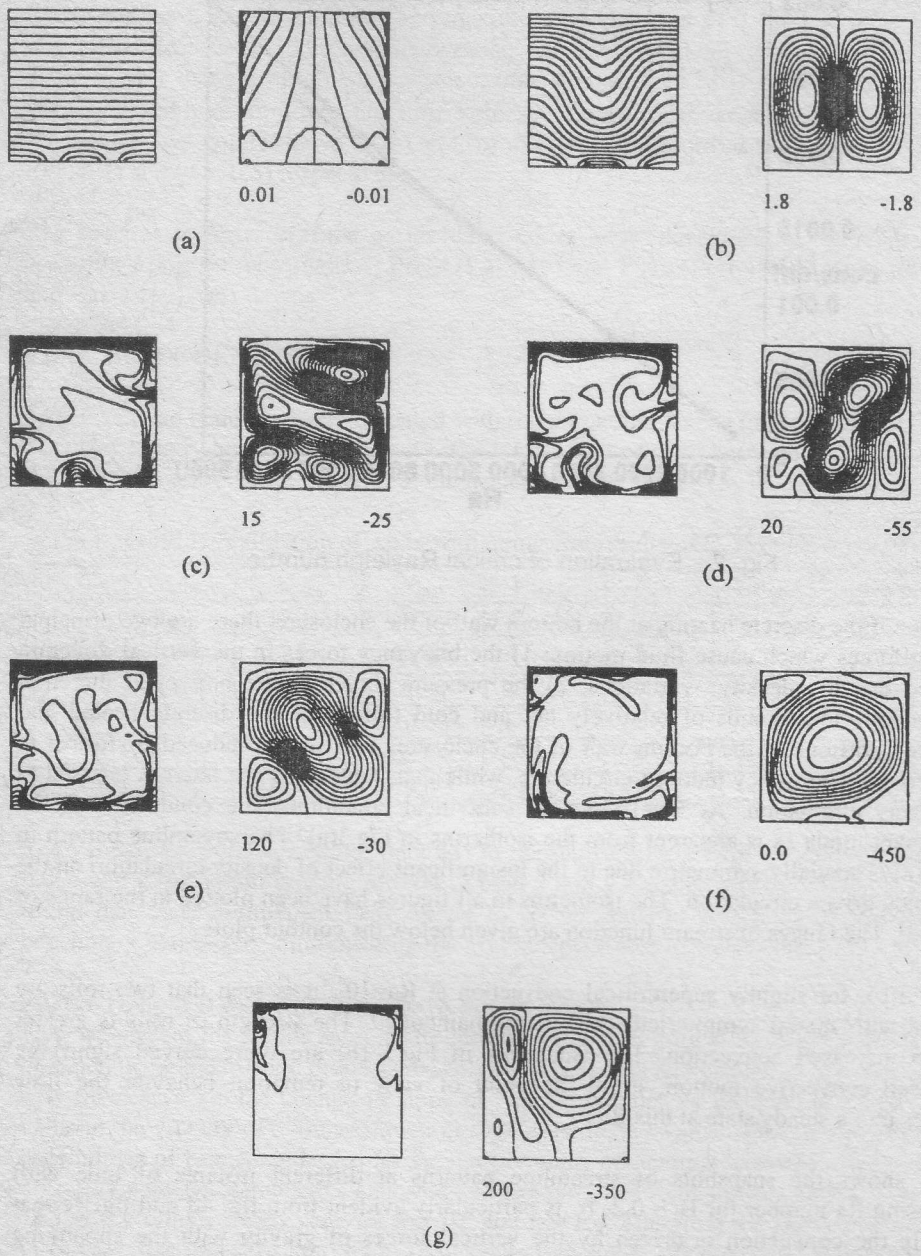


Fig. 3 Isotherms and Streamlines at an instant for different Ra at $H_l$=0.2 (a) Ra=$10^3$ (b) Ra=$10^4$ (c) Ra=$9*10^5$ (d) Ra=$1.4*10^6$ (e) Ra=$2.8*10^6$ (f) Ra=$2.24*10^7$ (g) Ra=$6.72*10^7$

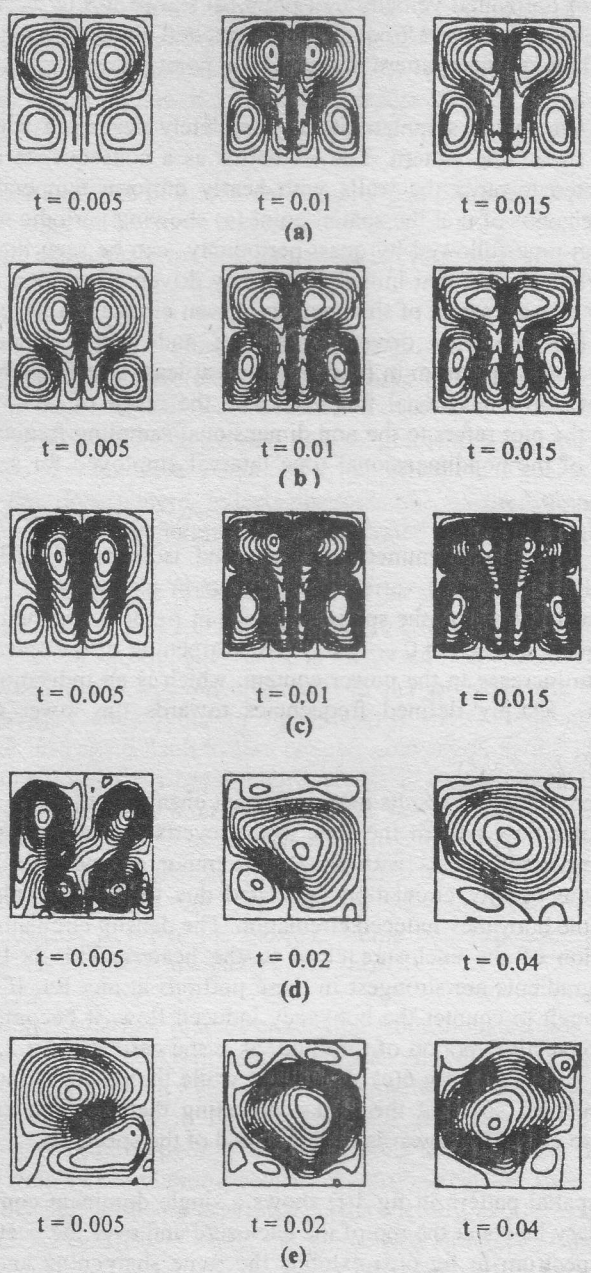


Fig. 4 Streamline pattern at $H_l$ = 0.2 at different instant of time for (a) Ra=$9*10^5$ (b) Ra=$1.4*10^6$ (c) Ra=$2.8*10^6$ (d) Ra=$2.24*10^7$ (e) Ra=$6.72*10^7$

From the time histories of horizontal velocity u at point (a) shown in Fig. 5, it is evident that with increase in Ra, more and more frequencies are excited along with an increase in the amplitude of fluctuations. Similar pattern is observed at point (b).

At $Ra=9*10^5$, (Fig. 3c) the spatial symmetricity is completely destroyed with the flow exhibiting multicellular streamline pattern. The isotherms as a consequence are heavily distorted and are deflected towards the walls with nearly uniform temperature in the interior. The temporal behavior of u at the spatial point (a) showing periodic motion with harmonics upto a certain time followed by quasi-periodicity can be seen in Fig. 5 (a) . This can be explained from the fact that initially buoyancy driven circulation is the main driving force but after a certain instant of time density driven circulation becomes strong enough to counteract the buoyancy driven circulation and hence temporal quasi-periodicity appears. The power spectrum in fig 6(a) shows at least five frequencies with a fairly broad spectrum of non-dimensional frequencies in the range of 0 — 0.05. The frequency $f_{max}$ shown in the plot refers to the non dimensional sampling frequency for the signal and is reciprocal of the nondimensional time interval employed for sampling the time series data.

At $Ra=1.4*10^6$ , there is spatial asymmetry of rolls and isotherms (Fig.3 (d)). The temporal variation of all the dynamic variables is similar in nature to $Ra=9*10^5$ flow except that the power spectrum of u at the spatial point (a) in fig 6(b), distinctly shows (i) the reduction in the frequency range to 0 — 0.025 (ii) Sharpening of the spectrum at the various peaks and (iii) an increase in the power content, which is an indication of power getting concentrated in sharply defined frequencies towards the lower end of the spectrum.

Further rise in Ra number to $2.8*10^6$ results in a significant change in the flow pattern (fig 3(e)). From a multicellular flow pattern the flow again reverts towards a state where a single dominant convective roll exists with small and minor secondary rolls. This is because at higher Ra, the density circulation generated due to alternate placement of heaters tends to counter the buoyancy induced circulation. The density circulation is strong only in the lower portion of the enclosure close to the heaters. This is because the horizontal temperature gradients are strongest in these portions at any Ra. If the density circulation is strong enough to counter the buoyancy induced flow, it becomes the main driving force causing convective motion of the fluid, as is the case at $Ra = 2.8*10^6$. The power spectrum of u at point (a) in fig 6(c) shows that while the power is increased, the spectrum becomes even more sharp at the peaks indicating that the frequencies while becoming distinct are also clustering towards the lower end of the spectrum.

At $Ra = 2.24*10^7$, the spatial pattern in fig 3(f) shows a single dominant convective roll with thin thermal boundary layers at the top of the enclosure and over the heated portions of the enclosure. The spectrum in fig 6(d) exhibits the same sharpening and clustering trend with increase in power.

Finally at $Ra = 6.72*10^7$ the isotherms are clustered at the top of the enclosure indicating that a very thin thermal boundary layer is formed at the top with temperature

nearly uniform in the entire enclosure (fig 3(g)). From the streamline pattern it is evident that in the lower portion of the enclosure the fluid velocities are much smaller than in the upper portion. Fig 6(e) shows the clustering and sharpening phenomenon of the spectrum at point (a). Thus it can be inferred that the density circulation suppresses higher frequencies.

From the time histories of horizontal velocity u at point (a) shown in Fig. 5, it is evident that with increase in Ra, more and more frequencies are excited along with an increase in the amplitude of fluctuations. Similar pattern is observed at point (b).

**Effect of heater length**

In order to establish the effect of heater length on the spatio-temporal dynamics, the numerical simulations were carried out for three heater lengths, namely $H_l$ = 0.15, 0.20, 0.25, keeping the number of heaters fixed and equal to 3. The basic effect of heater length is to alter the strength of horizontal density gradient $\partial\theta/\partial x$ in the vicinity of the heaters and to alter the surface area of thermal diffusion. Thus, at any given Ra and heater length $H_l$, the flow pattern reflects the outcome of the competition between vertical buoyancy forces, and the pressure forces generated due to horizontal density gradients.

Figures 7 and 8 depict the effect of heater length at a given instant of time for four values of Ra, namely $10^4$, $9*10^5$, $2.8*10^6$ and $2.24*10^7$. At lower Ra ($\leq 10^4$ ) the effect is hardly discernible (fig. 7a and fig. 8a). As Ra is increased from $10^4$ to $9*10^5$ (fig. 7b and fig. 8b) one can clearly make out the difference in the isotherm and streamline patterns. The spatial pattern of streamlines in fig 7b(i)-(iii) shows a change from less cellular to multicellular and again back to less cellular convection as the heater length is increased from 0.15 to 0.25. This is because an increase in heater length from 0.15 to 0.2 leads to enhanced convection due to an increase in the heating surface area. The effect of increase in area dominates the effect of simultaneous increase in the strength of density circulation, leading to the formation thermal plume like structures as seen in fig 8b(ii). As the heater length is further increased to 0.25 at same Ra and at the same time instant we find that the density circulation destroys the thermal plume like structure as seen in fig 8b(iii), leading to a less cellular flow pattern (fig 7b(iii)).

The formation of thermal plumes emanating from the heaters is a sign of strong vertical buoyancy and weak density circulation effects. At still higher Ra = $2.8*10^6$ , at $H_l$ = 0.15 the strong vertical buoyancy leads again to a multicellular flow pattern and thermal plume like structures as shown in fig 7c(i) and fig 8c(i) respectively. This flow pattern is destroyed as the heater length is increased to 0.2 and further to 0.25 (fig 7c(ii)-(iii)). The strength of density circulation becomes so strong that the flow is essentially driven by horizontal density gradients generated in the vicinity of the heaters. This is particularly evident from fig 8c(i)-(iii) where the plume like structure at the central heater for $H_l$ = 0.15 is flattened by density circulation at $H_l$ = 0.2 and at $H_l$ = 0.25. Similar trend is observed at Ra = $2.24*10^7$ (fig 7d and fig 8d).

The effects of buoyancy circulation and density circulation on the temporal dynamics are also brought about very clearly through figures 9a-9c. In fig 9a the effect of heater length at Ra = $9*10^5$ can be seen. In case (i) and (ii) (fig 9a) the buoyancy induced convective motion is dominant and the power spectrum of u at point (a) shows multiple dominant frequencies which are distinctly separated from one another. As the heater length is increased, the number of dominant frequencies reduces to two while the power of fluctuations is increased. At higher Ra = $2.8*10^6$ , fig 9b, it is observed that while the power is increased and the spectrum gets clustered due to the frequencies coming closer to each other, with increase in the heater length the frequencies at the lower end of the spectrum are also excited (fig 9b(iii)). Similar trend is observed at Ra = $2.24*10^7$ as shown in fig 9c.

## CONCLUSIONS

From the above numerical investigations it can be concluded that the spatio-temporal dynamics in an enclosure with discrete heating at the bottom is governed by two main parameters
1) the Rayleigh number 2) the length of the discrete heating portions $H_l$ . While the Ra number affects the vertical buoyancy, the placement of discrete heating portions generates horizontal density gradients and consequently an associated density circulation effect, which is affected by the length of the heating portions.

The spatial flow pattern at any given Ra and $H_l$ is an outcome of the competing effects of convection generated due to vertical buoyancy from the discrete heating surfaces and convective motion generated due to horizontal density gradient. The former results in a multicellular flow pattern with the formation of thermal plume like structures, while the latter results in a less multicellular flow with mostly one dominant convective roll. The buoyancy induced convection dominates for Ra < $9*10^5$ for all heater lengths while the density induced convection dominates for Ra > $9*10^5$ for all heater lengths. At Ra = $9*10^5$ buoyancy convection dominates for $H_l < 0.2$,
while density circulation dominates for $H_l \geq 0.2$

The temporal dynamics also exhibits strong dependance on Ra and a somewhat weaker influence of $H_l$ . At lower Ra the power spectrum of the time series data exhibits a fairly broad spectrum with distinct dominant frequencies sharing almost similar magnitude of power. With increase in Ra, the frequencies come closer to each other with peaks becoming sharper, the intensity of fluctuations also increases. With increase in heater length there is a small shift in the concentration of power towards the low frequency side of the spectrum, indicating that the density circulation causes less multicellular convection than buoyancy induced convection.

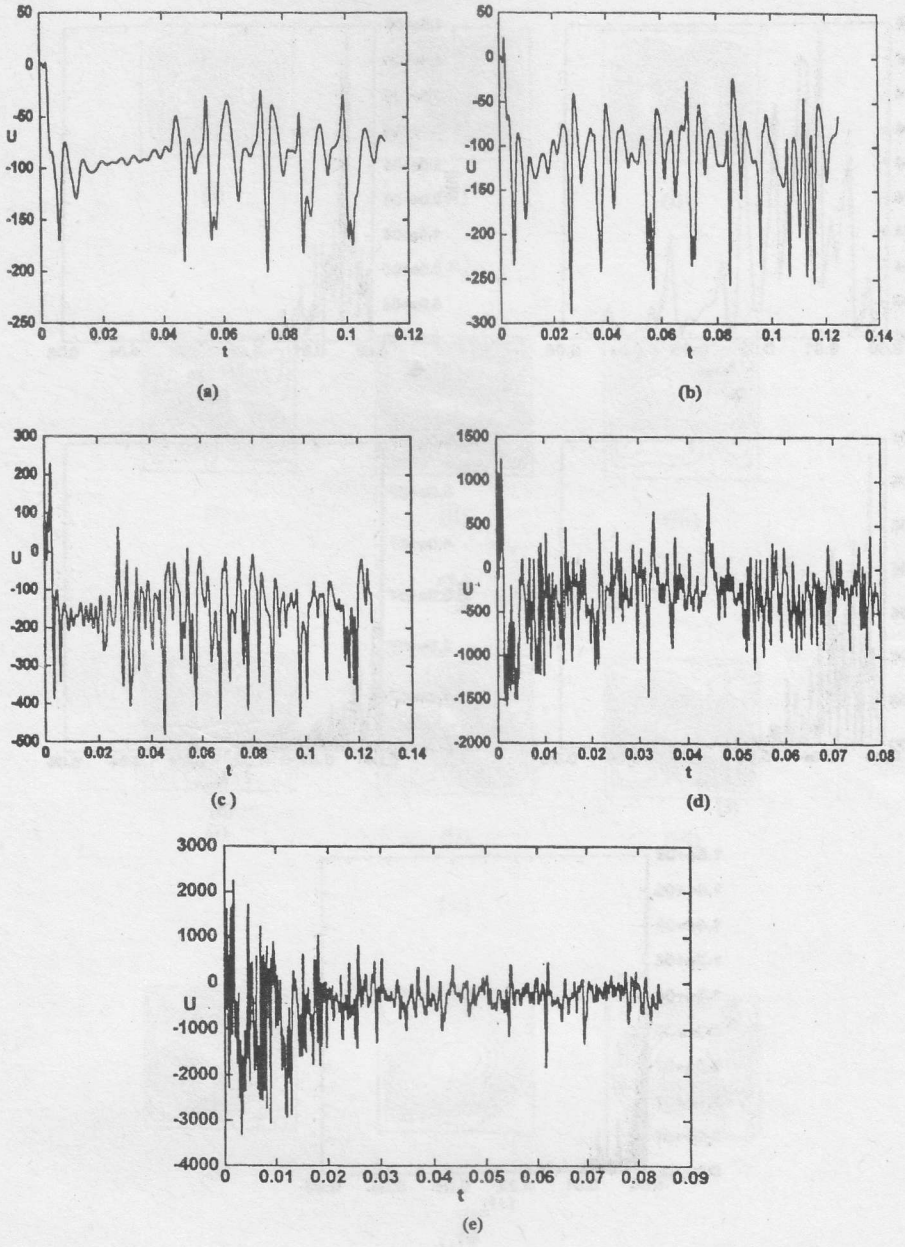


Fig. 5 Time histories of velocity u at point (a) at $H_l$ = 0.2 for (a) Ra=$9*10^5$ (b) Ra=$1.4*10^6$ (c) Ra=$2.8*10^6$ (d) Ra=$2.24*10^7$ (e) Ra=$6.72*10^7$

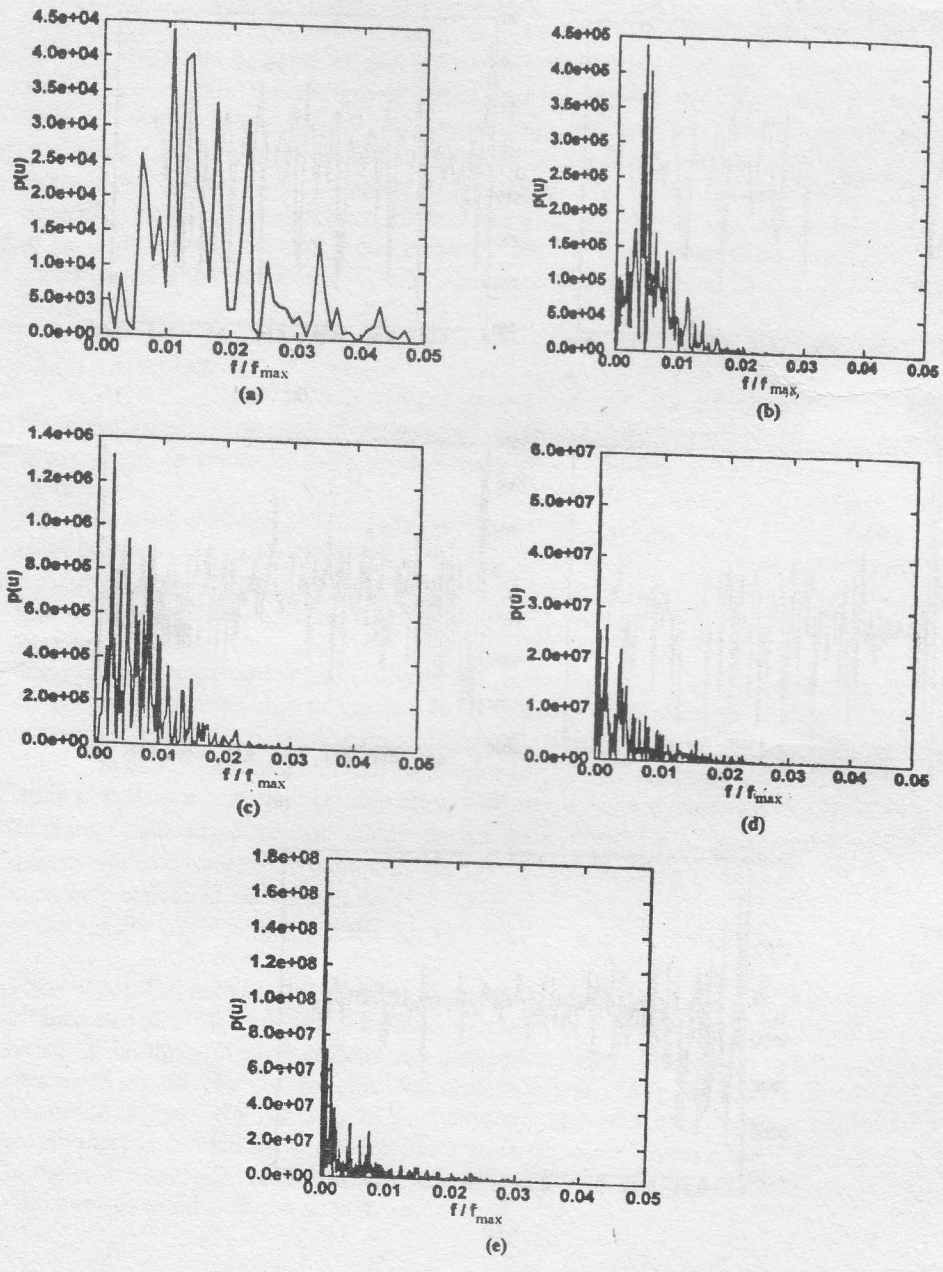


Fig. 6 Power spectrums of velocity u at point (a) at $H_l = 0.2$ for (a) $Ra=9*10^5$ (b) $Ra=1.4*10^6$ (c) $Ra=2.8*10^6$ (d) $Ra=2.24*10^7$ (e) $Ra=6.72*10^7$

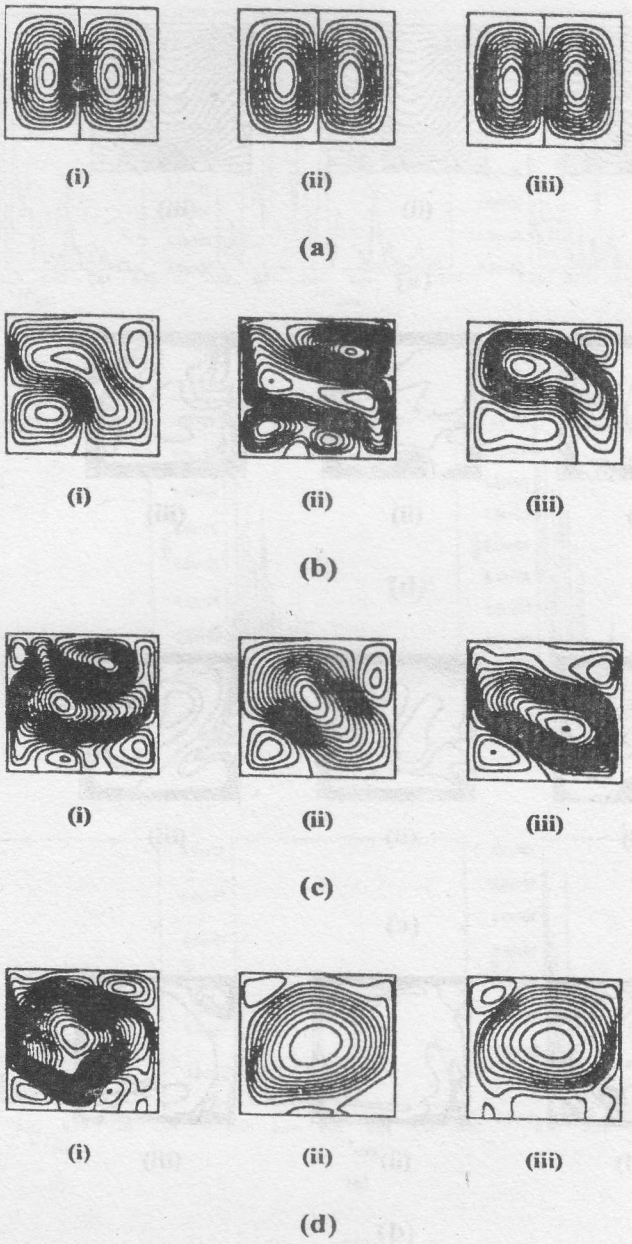


Fig. 7 Streamline patterns for (i) $H_l$ = 0.15 (ii) $H_l$ = 0.20 (iii) $H_l$ = 0.25 at (a) $Ra=10^4$ (b) $Ra=9*10^5$ (c) $Ra=2.8*10^6$ (d) $Ra=2.24*10^7$

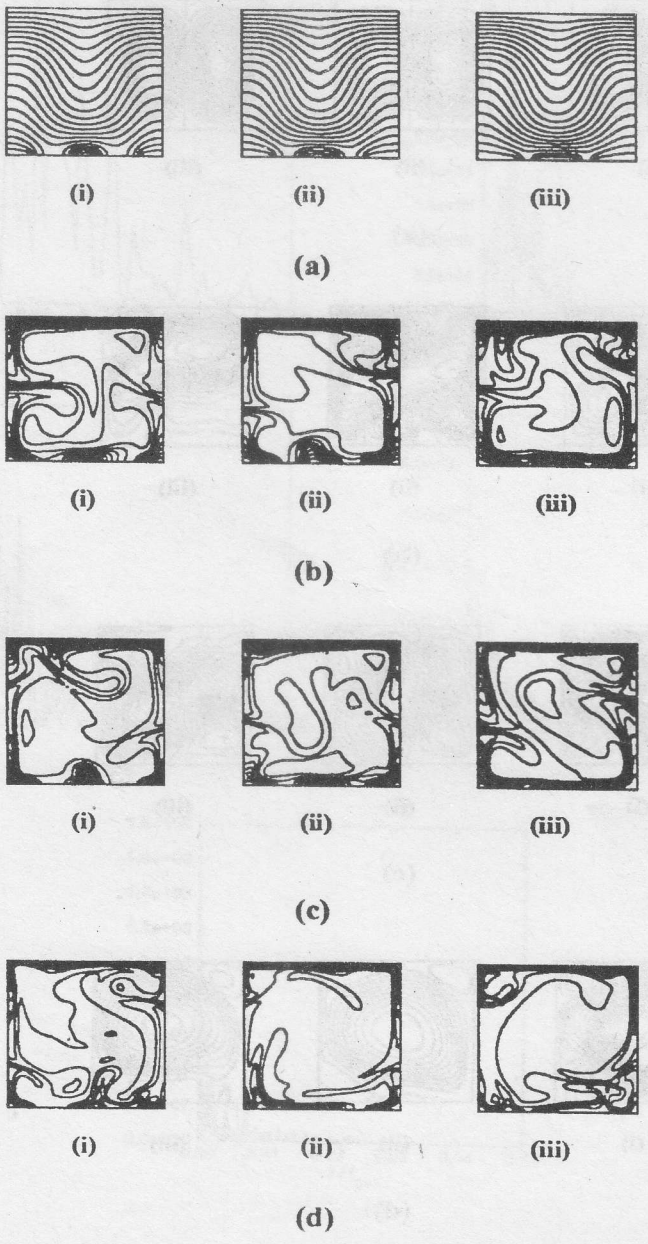


Fig. 8 Isotherms for (i) $H_l = 0.15$ (ii) $H_l = 0.20$ (iii) $H_l = 0.25$ at (a) $Ra=10^4$ (b) $Ra=9*10^5$ (c) $Ra=2.8*10^6$ (d) $Ra=2.24*10^7$

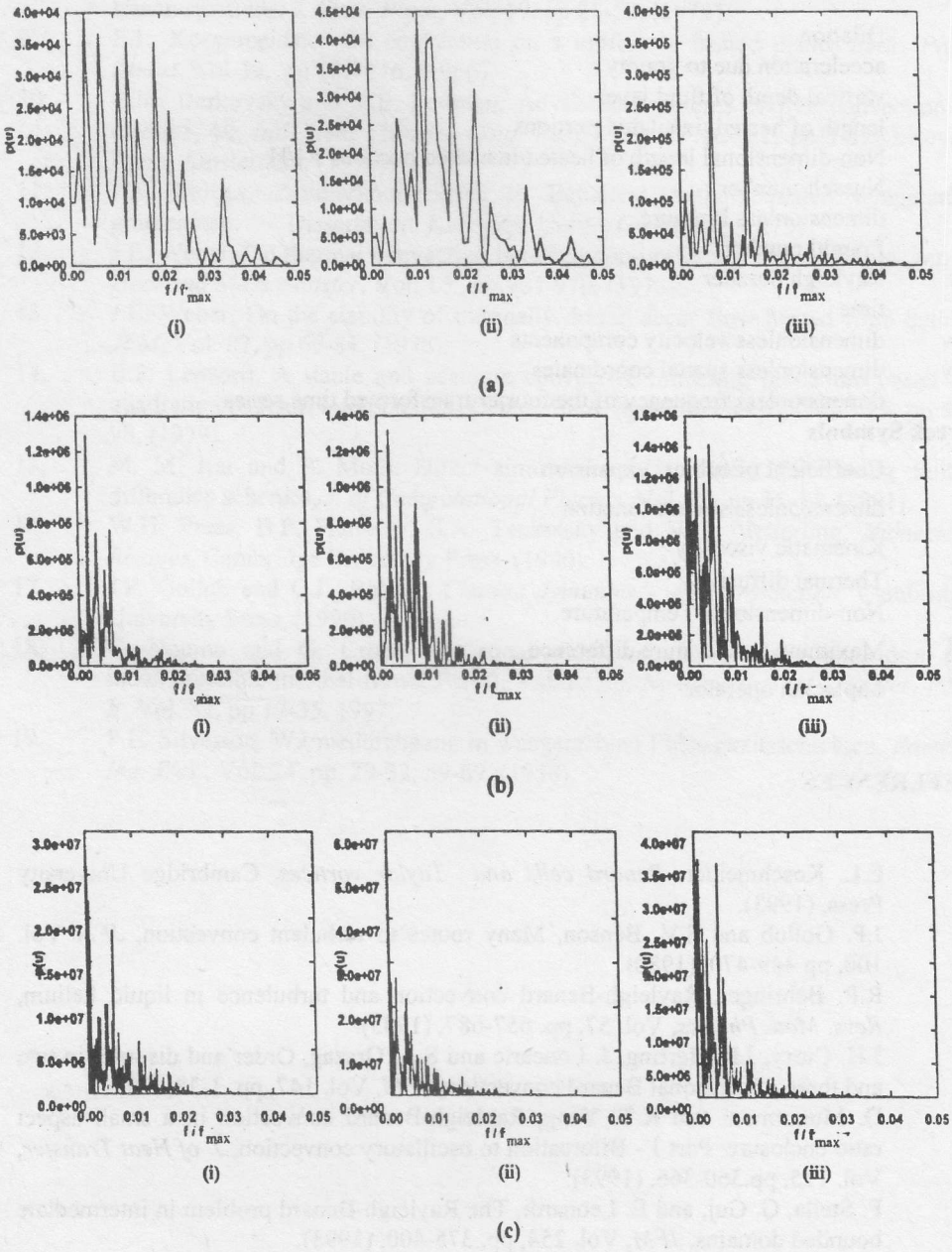


Fig. 9 Power spectrums of u at point (a) for (i) $H_l = 0.15$ (ii) $H_l = 0.20$ (iii) $H_l = 0.25$ at (a) $Ra=9*10^5$ (b) $Ra=2.8*10^6$ (c) $Ra=2.24*10^7$

## NOMENCLATURE

| | |
|---|---|
| D | Dilation |
| g | acceleration due to gravity |
| H | vertical depth of fluid layer |
| l | length of heated /insulated portions |
| $H_l$ | Non-dimensional length of heated/insulated portions = l/H |
| Nu | Nusselt number |
| P | dimensionless Pressure |
| Pr | Prandtl number |
| Ra | Rayleigh number |
| t | time |
| u, v | dimensionless velocity components |
| x, y | dimensionless spatial coordinates |
| f | dimensionless frequency of the fourier transformed time series |

**Greek Symbols**

| | |
|---|---|
| $\alpha$ | Coefficient of cubical expansion |
| $\psi$ | dimensionless stream-function |
| $\nu$ | Kinematic viscosity |
| $\kappa$ | Thermal diffusivity |
| $\theta$ | Non-dimensional Temperature |
| $\Delta T$ | Maximum temperature difference |
| $\nabla^2$ | Laplacian operator |

## REFERENCES


1. E.L. Koschmeider, *Benard cells and Taylor vortices*, Cambridge University Press, (1993).
2. J.P. Gollub and S.V. Benson, Many routes to turbulent convection, *JFM* Vol. 100, pp 449-470, (1980).
3. R.P. Behringer, Rayleigh-Benard convection and turbulence in liquid helium, *Revs. Mod. Physics*, Vol. 57, pp. 657-687, (1985).
4. J.H. Curry, J.R. Herring, J. Loncaric and S.A. Orszag, Order and disorder in two and three dimensional Benard convection, *JFM*, Vol. 147, pp. 1-38, (1984).
5. D. Mukutmoni and K.T. Yang, Rayleigh-Benard convection in a small aspect ratio enclosure: Part 1 - Bifurcation to oscillatory convection, *J. of Heat Transfer*, Vol. 115, pp.360-366, (1993).
6. F. Stella, G. Guj, and E. Leonardi, The Rayleigh-Benard problem in intermediate bounded domains, *JFM*, Vol. 254, pp. 375-400, (1993).
7. D. Ruelle, F. Takens and S.P. Newhouse, Occurrence of strange attractors near quasi-periodic flows on $T^m$, m>3, *Commun. Maths. Phys.*, Vol. 64, pp 35-40, (1978).

8. M.J. Feigenbaum, Quantitative universality for a class of nonlinear transformations, *J. Stats. Phys.*, Vol. 19, pp.25-52, (1978).
9. E.L. Koschmeider, On convection on a uniformly heated plane, *Beitr. Phys. Atmos.* Vol 39, pp 208-216, (1966).
10. B.M. Berkovsky and V.E. Fertman, Advanced problems of free convection in cavities, 4th *Intl. Heat Transfer Conf. Paris*, Vol. 4, NC 2.1, pp 1-12, Elsevier Press, Amsterdam, (1970).
11. J.A Srulijes, Zellularkoonvektren in Behältem mithorizentalen temperatur-gradienteen, Dissertation, Karlsruhe Univ. , Germany., (1979).
12. J.E. Weber, On thermal convection between non-uniformly heated planes, *Int. J. Heat and Mass transfer*, Vol. 16., pp 961-970, (1973).
13. J.E. Weber, On the stability of thermally driven shear flow heated from below, *JFM*, Vol. 87, pp 65-84, (1978).
14. B.P. Leonard, A stable and accurate convective modeling procedure based on quadratic upstream interpolation, *Comp. Meth. Appl. Mech Eng.*, Vol. 19, pp 59-98, (1979).
15. M. M. Rai and P. Moin, Direct simulations of turbulent flow using finite-difference schemes, *J. of Computational Physics*, Vol. 96, pp.15-53, (1991).
16. W.H. Press, B.P. Flannery, S.A. Teukolsky and W.T. Vetterling, *Numerical Recipes*, Cambridge University Press, (1990).
17. J.P. Gollub and G.L. Baker, *Chaotic dynamics - An introduction,* Cambridge University Press, (1990).
18. C. Nonino and G. Croce, An equal order velocity-pressure algorithm for incompressible thermal flows, Part 2: Validation, *Numerical Heat Transfer, Part B*, Vol. 32, pp 17-35, 1997.
19. P.L. Silveston, Wärmedurchgang in waagerechten Flüssigkeitsschichten, *Forsch. Ing. Wes.*, Vol. 24, pp. 29-32, 59-69, (1958).